



Article

Oral Delivery of mRNA by Liposomes Functionalized with Cell-Penetrating Peptides

Valerie Dürr¹, Sabrina Wohlfart², Tom Eisenzapf¹, Walter Mier², Gert Fricker¹  and Philipp Uhl^{1,*}¹ Institute of Pharmacy and Molecular Biotechnology, Heidelberg University, 69120 Heidelberg, Germany² Department of Nuclear Medicine, Heidelberg University Hospital, 69120 Heidelberg, Germany

* Correspondence: philipp.uhl@uni-heidelberg.de; Tel.: +49-6221-54-4170

Abstract: Lipid nanoparticles, including liposomes, have emerged as promising vehicles for the delivery of a variety of therapeutics. Several formulations have been approved and are used in medical practice—the COVID-19 mRNA vaccines represent the most recent milestone. Achieving effective oral delivery would elevate the potential of these formulations. Therefore, this study investigates the oral application of mRNA using liposomes as a nanocarrier system. A cyclic cell-penetrating peptide was coupled to the liposomal surface to allow uptake into the intestinal mucosal cells. The liposomes were loaded with mRNA (up to 112 µg/mL) and characterized in terms of their size (Z-average; 135.4 nm ± 1.1 nm), size distribution (polydispersity index (PDI); 0.213 ± 0.007 nm), surface charge (2.89 ± 0.27 mV), structure, lamellarity (multilamellar liposomes), and cargo capacity (>90%). The impact of freeze-drying and long-term storage of liposomal formulations was examined, and in vitro experiments on Caco-2 cells were conducted to evaluate the cytotoxicity of the liposomal formulations and demonstrate the uptake of the liposomes into cells. The efficiency of the formulations could be proven in vitro. When compared to control liposomes and 1,2-dioleoyl-3-trimethylammonium propane (DOTAP)-liposomes, the new formulations exhibited significantly enhanced uptake in Caco-2 cells, an immortalized epithelial cell line. Moreover, the cytocompatibility of the formulations could be proven by the absence of cytotoxic effects on the viability of Caco-2 cells. Hence, this liposomal drug delivery system holds significant promise for the oral delivery of mRNA.



Citation: Dürr, V.; Wohlfart, S.; Eisenzapf, T.; Mier, W.; Fricker, G.; Uhl, P. Oral Delivery of mRNA by Liposomes Functionalized with Cell-Penetrating Peptides. *Appl. Nano* **2023**, *4*, 293–308. <https://doi.org/10.3390/applnano4040017>

Academic Editors: Anthony William Coleman and Giacomo Dacarro

Received: 18 September 2023

Revised: 3 November 2023

Accepted: 7 November 2023

Published: 9 November 2023



Copyright: © 2023 by the authors. Licensee MDPI, Basel, Switzerland. This article is an open access article distributed under the terms and conditions of the Creative Commons Attribution (CC BY) license (<https://creativecommons.org/licenses/by/4.0/>).

Keywords: liposomes; oral delivery; cell-penetrating peptides; mRNA

1. Introduction

Nanocarriers have been examined as drug delivery systems for decades [1]. In the meantime, a few formulations have been approved by the authorities and are used in medical practice, with the most recent milestone being the development of mRNA vaccines to fight the COVID-19 pandemic [2]. These vaccines exemplarily demonstrate how LNPs can serve as carriers for the delivery of nucleic acids. Nucleic acid therapeutics offer great potential for the prevention, treatment, and cure of various diseases [3]. A major challenge is to deliver the functional nucleic acid to the target structure without degradation in biological fluids [4]. The second major hurdle mRNA therapeutics encounter is their uptake, beyond their accumulation in the target tissue. Therefore, a carrier is mandatory because mRNA cannot easily penetrate cellular membranes [5]. To date, all lipid nanoparticle (LNP)-based drugs must be administered parenterally, as oral administration is restricted by several limitations, such as the degradation and destabilization of active ingredients by the low pH in the stomach, as well as enzymes and shear forces in the gastrointestinal tract, leading to negligible oral bioavailability [4]. However, it is of great interest to transfer the applicability of LNPs to oral application, as oral administration is still the preferred route for drug administration. It is convenient, well accepted, and painless, resulting in high patient compliance [6]. In addition, oral application can be performed by the patient itself [7]. However, until now, this route of administration has barely been suitable for

drugs such as nucleic acids due to their negligible oral bioavailability (based on the low stability of biologics in the gastrointestinal tract (GIT), due to not sufficient transport across the intestinal barrier and low uptake into the blood) and the intestinal epithelial cells acting as a physical barrier [8]. In addition, oral administration of drugs encounters a steric barrier, the mucus layer, which is largely composed of densely glycosylated proteins that are constantly secreted and excreted through the GIT. Furthermore, the transit time of orally administered drugs must be slow enough to allow interaction with and subsequent diffusion through the mucus. Oral delivery of macromolecular drugs is further limited as they are highly susceptible to enzymatic degradation in the gastrointestinal tract. The low pH in the stomach causes protonation, potential unfolding, and structural changes in these compounds. In addition, enzymes can render biologics therapeutically ineffective by causing irreversible chemical or biological changes [9]. Therefore, the oral delivery of macromolecular drugs is favorable but, up to date, difficult to realize and has been successful in only a few applications. For a long time, the immunosuppressant cyclosporine A represented the only peptide therapeutic with drug-like oral bioavailability [10]. The original oil-based oral formulation (Sandimmun[®]) was improved by a microemulsion formulation (Neoral[®]) due to high pharmacokinetic variability [11]. Recently, two oral formulations of peptide therapeutics could be approved by the European Medicine Agency (EMA) and the Food and Drug Administration (FDA). First, Rybelsus[®] oral semaglutide with salcaprozate sodium as a permeation enhancer enables once-daily oral administration of semaglutide to avoid injections in the treatment of people with type 2 diabetes [12]. Second, the enteric-coated capsule MYCAPSSA[®] enables oral administration of the peptide therapeutic octreotide [13]. Despite these examples of successful oral delivery, most approaches studied have not been successful to date. The characteristics of liposomes, an early version of LNPs, make them highly versatile drug delivery systems, as they allow the delivery of both hydrophobic and hydrophilic molecules, including small molecules, proteins, and nucleic acids [14,15]. Liposomes were the first nanocarriers to successfully progress from being a concept to clinical application [16]. While liposomes form a simple lipid bilayer, later generations of LNPs, including solid lipid nanoparticles, nanostructured lipid carriers, and cationic lipid–nucleic acid complexes, have a more complex composition and structure. These more complex nanoparticles, which have improved physical stability and enable time- and location-dependent delivery of drugs, can therefore potentially be applied for drug delivery in a broad range of diseases [5]. However, the mucus represents a viscous layer lining the entire GIT. This barrier limits oral delivery of macromolecular drugs. It is composed of proteoglycan-coated mucin protein, secreted by the goblet cells of the GIT epithelia [17,18]. It exhibits a high turnover rate and is thus part of mucosal immunity by trapping and removing foreign structures before they can reach the underlying epithelia. This process is called mucosal clearance and further reduces the oral bioavailability of specific drugs [19,20]. To overcome this hurdle, liposomes can be modified to achieve mucus-penetrating or mucus-adhesive properties by coating them with hydrophilic or cationic oligomers or polymers, preferentially cell-penetrating peptides (CPPs) [21]. Today, a variety of CPPs exist; however, in this study, an arginine-rich CPP was selected since the literature describes them as exceptionally low- to non-toxic [22]. Further, a cyclic peptide was selected for this project because previous work showed increased stability of cyclic CPPs compared to linear CPPs in the gastrointestinal fluids [23,24]. In this study, the concept of oral mRNA administration using CPP-modified liposomes as a carrier system was investigated. The cell-penetrating peptide was coupled to the liposomal surface to promote uptake into intestinal mucosal cells. Liposomal preparation was performed by dual asymmetric centrifugation (DAC). The liposomes were loaded with mRNA and subsequently characterized in terms of size, size distribution, surface charge, structure, lamellarity, and entrapment efficiency. The impact of freeze-drying and long-term storage on the liposomal formulations was examined, and *in vitro* experiments on Caco-2 cells were conducted to evaluate the cytotoxicity of the liposomal formulations and demonstrate liposomal uptake.

2. Materials and Methods

2.1. Materials

Lecithin was purchased from AppliChem GmbH (Darmstadt, Germany); glyceryl-caldityl tetraether lipid (GCTE) was isolated from *S. acidocaldarius* as described by Uhl et al. [17]. The cyclic CPP was synthesized in our lab as described previously by Uhl et al., (2021) [25]. DOTAP and rhodamine-labeled phospholipids were obtained from Avanti Polar Lipids (Alabaster, AL, USA). Ceramic beads (1.0–1.2 mm) were obtained from Sigmund Lindner GmbH (Warmensteinach, Germany). Green fluorescent protein (GFP)-mRNA was purchased from RiboPro B.V. (Oss, The Netherlands); Lipofectamine MessengerMAX[®] was obtained from Thermo Fisher Scientific (Waltham, MA, USA); cholesterol and all solvents were purchased from Sigma Aldrich (Taufkirchen, Germany). All remaining chemicals were purchased from standard commercial suppliers at the highest available grade.

2.2. Methods

2.2.1. Liposome Preparation by Thin-Film Hydration Method

Liposomal compositions were chosen according to optimized lipid ratios described previously by Uhl et al. [25]. Liposomes were prepared by the thin-film method, followed by rehydration and dual asymmetric centrifugation (DAC). For this purpose, lipids were dissolved in an organic solvent mixture of chloroform/methanol in a ratio of 9:1 (*v/v*), and lipid stocks were stored at $-20\text{ }^{\circ}\text{C}$. The required volumes for the desired liposome composition were mixed in 2 mL microtubes according to Table 1, respectively, if not indicated differently. The lipid film was formed by evaporating the organic solvents on a heat block at $50\text{ }^{\circ}\text{C}$ under a nitrogen stream. To ensure the complete removal of organic solvents, the film was finally dried in a vacuum chamber. To enhance shear forces and thus obtain homogenous particle sizes, ceramic beads were added during the centrifugation process. Afterwards, the liposomes were formed by hydrating the lipid film. Two runs were performed with the dual asymmetric centrifuge ZentriMix 380 R (Andreas Hettich GmbH and Co. KG, Tuttlingen, Germany) at $20\text{ }^{\circ}\text{C}$ and 2500 rpm. In the first run of 15 min, 28 μL of GFP-mRNA were added to the dried lipid film, leading to a final concentration of either 40 $\mu\text{L}/\text{mL}$ mRNA or 112 $\mu\text{g}/\text{mL}$ mRNA, depending on the experiment. The mRNA was diluted in water for injection. In the second run of 5 min, the five-fold mass of water for injection was added. In the last step, water for injection was added to reach a final volume of 250 μL of liposomes, and the sample was quickly vortexed for homogenization. For empty liposomes, water for injection was used in all steps.

Table 1. Lipid composition of liposome formulations.

[mol%]	Control	DOTAP	CPP	GCTE	CPP-GCTE
Lecithin	90	85	89	85	84
Cholesterol	10	10	10	10	10
DOTAP	0	5	0	0	0
CPP	0	0	1	0	1
GCTE	0	0	0	5	5
Lipid mass [mg/mL]	72.28	72.20	74.44	75.76	77.92

2.2.2. Size and Size Distribution

The size (Z-average) and size distribution, described by the polydispersity index (PDI), of liposomes were determined by photon correlation spectroscopy.

Liposomes were diluted 1:1000 in phosphate buffered saline (PBS) in a single-use polystyrene cuvette and measured with Zetasizer Nano ZS (Malvern Panalytical, Malvern, UK). The default settings of the automatic mode of the Zetasizer are shown in Table 2.

Table 2. Settings of Zetasizer Nano ZS for liposomal characterization.

Parameter	Setting
Number of measurements	3
Run duration	10 s
Number of runs	10
Equilibration time	60 s
Refractive index solvent	1.330
Refractive index polystyrene cuvette	1.590
Viscosity	0.8872 mPa·s
Temperature	25 °C
Dielectric constant	78.5 F/m
Backscattering mode	173°
Voltage selection	Automatic
Equation	Smoluchowski equation

2.2.3. Zeta Potential

The zeta potential was measured using the Zetasizer Nano ZS. Liposomes were diluted 1:20 in buffer (50 mM potassium dihydrogen phosphate, pH 7.4). An equilibration time of 60 s was set, and three measurements with 20 runs were performed.

2.2.4. Cryo-Transmission Electron Microscopy (Cryo-TEM)

Cryo-TEM imaging was performed at the Center of Biopharmacy at the University of Basel. The liposomes were prepared for cryo-TEM by dilution to a lipid concentration of 5 mg/mL. Afterwards, 4 µL aliquots of CPP- and GCTE-liposomes were adsorbed onto a holey carbon-coated grid (Lacey, Tedpella, Redding, CA, USA). Subsequent blotting was performed with Whatman Grade 1 filter paper and vitrified into liquid ethane at −180 °C (Leica GP2 plunger, Leica microsystems, Austria). Afterwards, the frozen grids were transferred onto a Talos 200 electron microscope (FEI, Peabody, MA, USA) using a Gatan 626 cryo-holder (GATAN, Pleasanton, CA, USA). Imaging was performed at an accelerating voltage of 200 kV using a low-dose system (40 e⁻/Å²), and the sample was kept at −175 °C. Defocus values were −2 to 3 µm. The recording of the images was performed on a 4K × 4K Ceta CMOS camera.

2.2.5. Encapsulation Efficiency

The amount of mRNA encapsulated in liposomes was quantified indirectly by the determination of free mRNA using the Quant-iT[®] RiboGreen[®] RNA Assay Kit obtained from Thermo Fisher Scientific Inc. (Waltham, MA, USA). For this, 25 µL of liposome formulation were diluted with 75 µL of TE buffer (Tris-EDTA buffer, provided by the RiboGreen[®] assay). For the resulting 100 µL sample, the RiboGreen[®] assay was applied, and the amount of free mRNA was detected according to the manufacturer's instructions. Fluorescence measurement was performed using a plate reader (excitation 485 nm and emission 535 nm). mRNA content was determined by subtracting the amount of non-encapsulated mRNA from the initial mRNA amount. Statistical significance was determined by a one-way ANOVA, followed by Dunnett's multiple comparisons test to compare all formulations to unmodified liposomes.

2.2.6. Long-Term Storage Stability by Freeze-Drying

To enable long-term storage stability, liposomal formulations were freeze-dried. The residual moisture of the lyophilizates was determined, and the impact of freeze-drying and storage conditions on liposomal characteristics was analyzed.

To analyze liposomal stability at lyophilization and after subsequent long-term storage, the following liposomal formulations were tested: Control liposomes, 1 mol% CPP-liposomes, and 5 mol% DOTAP-liposomes with 40 µg/mL GFP-mRNA. Sucrose was used as a lyoprotectant in a concentration of 500 mM, as described previously by Uhl et al. [26],

and was added to liposomal formulations after preparation. Liposomal characteristics (size and PDI) were measured both before and after the addition of sucrose. The zeta potential was determined from the samples containing the lyoprotectant. Liposomal formulations were partitioned into 50 μ L aliquots for lyophilization using the freeze dryer Epsilon 2–4 LSCplus (Martin Christ Gefriertrocknungsanlagen GmbH, Osterode am Harz, Germany), and the process was run as follows: (I) Freezing stage: The samples were cooled down to -40 °C for 2 h and held at this temperature for 4 h. (II) Primary drying stage: The vacuum was drawn to 0.1 mbar over 1 h and held for 24 h. (III) Secondary drying stage: The vacuum was drawn to 0.01 mbar over 2 h, and the temperature was steadily increased from -40 °C to 0 °C. The settings were then held for 40 h for the secondary drying stage. The residual moisture content of lyophilizates was determined from the sample weight loss after heating at 74 °C using a moisture analyzer. Statistical significance was determined by a one-way ANOVA, followed by the Dunnett's multiple comparisons test to compare for each formulation, respectively, the characteristics with and without the addition of the lyoprotectant as well as before and after lyophilization.

For stability analyses, the lyophilizates were stored at -20 °C, and the remaining liposomal dispersions of the formulations used for lyophilization were stored at room temperature. The size and PDI of both the lyophilizates and the liposomal dispersion were determined using a Zetasizer Nano ZS at various time points post-lyophilization: (0) directly after lyophilization, (I) 1 month post-lyophilization, and (II) 2 months post-lyophilization. For this, lyophilizates were resuspended in the same volume of solvent as pre-lyophilization (50 μ L of water for injection). Statistical significance was determined by a one-way ANOVA, followed by Tukey's multiple comparisons test to compare properties with and without freeze-drying and storage time within each formulation.

2.2.7. In Vitro Studies

Cell Culture

To model the human intestinal epithelial barrier, the immortalized cell line of human colorectal adenocarcinoma cells, colon-carcinoma-2 (Caco-2) cells, from passages 30 to 50, was used. The cell line was obtained from the Leibniz Institute DSMZ-German Collection of Microorganisms and Cell Cultures, Braunschweig, Germany. Caco-2 cells were cultivated in Dulbecco's Modified Eagle Medium (DMEM, Thermo Fisher Scientific Inc., Waltham, MA, USA) supplemented with 10% fetal bovine serum (FBS, Bio and Sell GmbH, Feucht, Germany), 1 mM sodium pyruvate (Thermo Fisher Scientific Inc., Waltham, MA, USA), 1% L glutamine (Sigma-Aldrich, St. Louis, MO, USA), 1% penicillin-streptomycin (Sigma-Aldrich, St. Louis, MO, USA), and 1% non-essential amino acids (Biochrom GmbH, Berlin, Germany).

Thawing Cells

Cells from liquid nitrogen storage were kept at room temperature for 2 min and then thawed in a water bath at 37 °C. Cells were transferred to a 15 mL falcon with 10 mL of prewarmed (37 °C) complete medium. After centrifugation for 10 min at $400\times g$, the supernatant was removed, and the cell pellet was resuspended in 10 mL of fresh complete medium. The cell suspension was transferred to a 75 cm² cell culture flask.

Cultivating Cells

Cells were cultivated at standard cell culture conditions (37 °C in an atmosphere of 95% ambient air, 5% CO₂, and 90% humidity) in 75 cm² cell culture flasks with 10 mL of complete medium. To keep cells in culture, subcultures were taken when cells reached 80% confluency. For this, the medium was removed, and cells were washed with 5 mL of prewarmed PBS and subsequently incubated with 2.5 mL of trypsin-EDTA (Sigma-Aldrich, St. Louis, MO, USA) for 5 min in the incubator to be detached. To stop the reaction, 5 mL of complete medium were added. To remove all trypsin, the cell suspension was centrifuged for 4 min at $400\times g$ so that the supernatant could be removed, and the cell pellet was resuspended in 5 mL of fresh medium. To keep cells in culture, usually cells were split 1:20.

Cell Counting

Cell concentrations were determined by counting cells using a Neubauer chamber. For this, cell suspensions were mixed with trypan blue in a 1:1 ratio, and all four squares were counted.

Cytotoxicity Studies

All incubations took place in standard cell culture conditions (37 °C, 95% ambient air, 5% CO₂, 90% humidity). In a 96-well plate, 10⁵ cells per well were seeded in 100 µL of medium and incubated overnight. On the second day, the medium was removed, and the cells were washed with 200 µL of PBS. Subsequently, the cells were incubated with 100 µL of the respective treatment for 4 or 24 h. Liposomes were diluted in complete medium or medium without supplements, depending on the experiment. For the negative control, cells were treated with 1% Triton X-100, and for the positive control, cells were incubated with the same medium used for liposome dilutions. After removing the supernatant, the cells were incubated for 2 h with 100 µL of PrestoBlue[®] working solution (1:10 in medium). To diminish the background fluorescence signal, blank samples (wells without cells but with 100 µL of PrestoBlue[®] working solution) were used for subtraction of the signal from the final test values. The reducing environment of viable cells modifies the PrestoBlue[®] reagent so that it becomes highly fluorescent. Thus, cell viability could be assessed by measuring the fluorescent signal on a plate reader at a wavelength of 590 nm with an excitation wavelength of 560 nm. Statistical significance was determined by a one-way ANOVA, followed by the Dunnett's multiple comparisons test to compare each group to the positive control corresponding to 100% cell viability.

Cellular Uptake of Liposomes

Caco-2 cells were seeded in a 96-well plate 24 h before the experiment to reach 80% confluency. The cells were washed with PBS and incubated for 1 h with 100 µL of treatment diluted in PBS. Here, liposomal formulations were fluorescently labeled with 1 mol% of a rhodamine-phospholipid conjugate, and a GFP-mRNA with a fluorescent dye (AZDye488) was used. After treatment incubation, the supernatants were collected in a 96-well plate for analysis of free liposomes, and the cells were washed with PBS twice. To determine the quantity of liposomes taken up, cells were lysed by a 15-minute incubation with 1% Triton X-100 in PBS at 37 °C (method 1). To avoid background signaling, cell debris was removed by a 5-minute centrifugation at 14,000 rpm. Additionally, cellular uptake of liposomes was determined directly without cell lysis but with intact cells covered with phenol-red-free medium (method 2). The amount of free and taken-up liposomes was determined by the quantification of the fluorescence signal of rhodamine. The signal was measured on a plate reader at a wavelength of 590 nm with an excitation wavelength of 540 nm, and concentrations were obtained via calibration lines of the respective liposomes. The mRNA was quantified via its fluorescence tag AZDye488 at a wavelength of 535 nm with an excitation wavelength of 485 nm. Furthermore, the uptake was visualized with a fluorescence microscope (Keyence BZ-X800 Benchtop Microscope, Keyence Deutschland GmbH, Neu-Isenburg, Germany). In addition to liposomal formulations, cells were treated with Lipofectamine (prepared according to the manufacturer's instructions) as a positive control. The cells were washed with PBS twice after treatment incubation and were covered with phenol-red-free medium. Phase contrast and fluorescence imaging were performed. Rhodamine was detected at 590 nm with an excitation wavelength of 540 nm to visualize liposomes, and the GFP-mRNA was visualized by detecting its fluorescent dye at 535 nm with an excitation wavelength of 485 nm. Statistical significance was determined by a two-way ANOVA, followed by the Dunnett's multiple comparisons test to compare CPP- and DOTAP-liposomes to control liposomes of the respective concentrations.

3. Results

3.1. Liposome Preparation and Characterization

Various liposomal formulations were prepared by DAC and subsequently characterized. First, the production parameters and liposome compositions were optimized, followed by the characterization of the formulations with respect to size, PDI, and zeta potential, as well as encapsulation efficiency, structure, and lamellarity.

To prepare liposomes, a thin lipid film was rehydrated by DAC, and shear forces were enhanced by adding ceramic beads. Since the optimal number of beads to achieve small and homogenous particles varies between different formulations, two bead amounts were tested: a bead number equivalent to five times the lipid mass and a bead number equivalent to ten times the lipid mass.

Lower PDIs, i.e., more homogenous particles, were obtained by using five times the lipid mass of beads for control liposomes (0.198 ± 0.004) and CPP-liposomes (0.231 ± 0.004), while using twice the number of beads resulted in smaller and more homogeneous DOTAP-liposomes (0.196 ± 0.015 ; Figure 1A). The zeta potential is not affected by the number of beads (Figure 1B). As expected, control liposomes had a negative zeta potential (-4.15 ± 0.20 mV), and CPP-liposomes had a positive zeta potential (2.45 ± 0.21 mV). The liposomal formulations loaded with GFP-mRNA were characterized by their particle size, PDI, and zeta potential. Liposome preparation by DAC enabled the production of liposomes with reproducible size, PDI, and zeta potential (Figure 1C). GCTE-CPP-liposomes displayed the largest particles of 153.0 nm, followed by CPP-liposomes with 135.4 nm, and control, DOTAP-, and GCTE-liposomes with sizes ranging from 104.8 to 115.1 nm. The PDI for the liposome formulations was <0.220 , indicating an acceptable size distribution (Figure 1C and Figure S1 for the size distribution of CPP-liposomes). Furthermore, liposome formulations without cationic lipids exhibited negative zeta potentials between -4.62 mV (GCTE-liposomes) and -5.94 mV (control liposomes), whereas liposomes with cationic lipids exhibited positive surface charges (CPP-liposomes: 2.89 ± 0.27 mV, GCTE-CPP-liposomes: 3.34 ± 0.15 mV, DOTAP-liposomes: 2.45 ± 0.40 mV; Figure 1D). Loading with different concentrations of mRNA (40 $\mu\text{g}/\text{mL}$ and 112 $\mu\text{g}/\text{mL}$) demonstrated that these mRNA concentrations do not negatively influence liposomal characteristics (size, PDI; Figure S2). For control liposomes, the mRNA concentrations showed no impact on liposomal characteristics, while for CPP-liposomes, increasing the mRNA concentration indeed resulted in smaller and more homogenous particles (indicated by lower PDI).

3.2. Structure, Lamellarity, Encapsulation Efficiency, and Stability in Simulated Gastric and Intestinal Fluids

Furthermore, the structure and lamellarity of GFP-mRNA-loaded CPP- and GCTE-liposomes were determined by cryogenic transmission electron microscopy (cryo-TEM) (Figure 2A), which showed primarily bi- and multilamellar but also, to a lesser extent, multivesicular particles. CPP-liposomes had a spherical morphology, while GCTE-liposomes had partially oval and deformed shapes. The formation of primarily bi- and multilamellar as well as multivesicular liposomes can be explained by the preparation method of liposomes, more precisely by the dual asymmetric centrifuge used. Previous work in our lab showed that using the dual asymmetric centrifuge ZentriMix 380R (Andreas Hettich GmbH and Co. KG, Tuttlingen, Germany), which was used in this project for the preparation of liposomes, leads to uni-, bi-, and multilamellar particles, while the SpeedMixer (DAC150FVZ Hauschild Engineering GmbH and Co. KG, Hamm, Germany) mainly forms unilamellar liposomes [26].

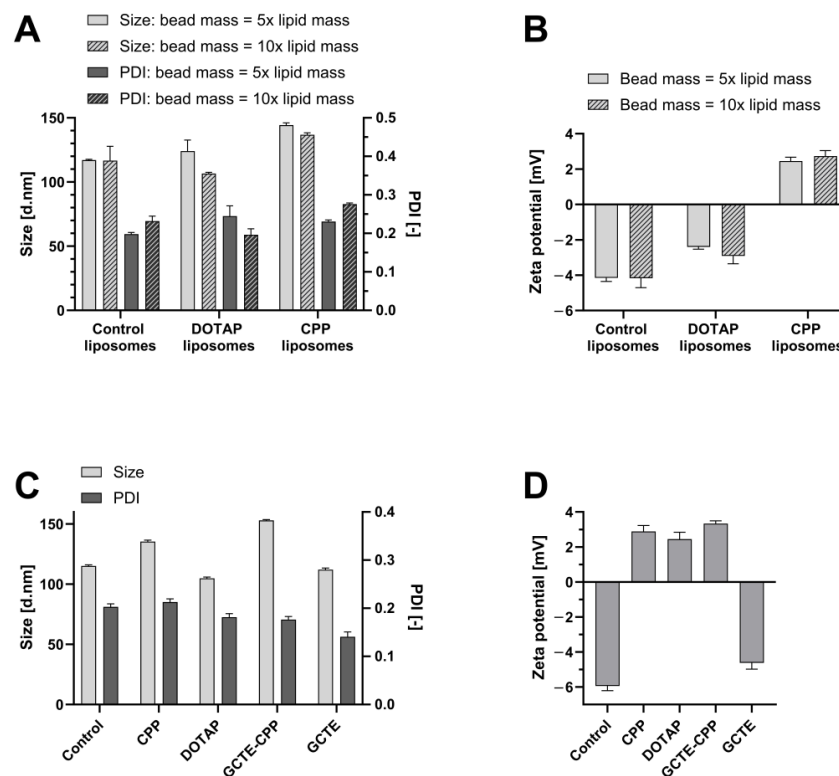


Figure 1. (A,B) Bead amount optimization: (A) Liposome particle size (Z-average) and PDI, and (B) zeta potential using different amounts of beads in the preparation of empty liposomes (bead amounts of five times of the lipid mass and ten times of the lipid mass). Control liposomes, 1 mol% DOTAP-liposomes, and 1 mol% CPP-liposomes were tested. Bars represent the mean ($n = 3$) \pm SEM. (C,D): Characterization of liposomes containing 40 µg/mL GFP-mRNA. (C) Size and PDI, and (D) Zeta potential of liposomes (control liposomes, 1 mol% CPP-liposomes, 5 mol% DOTAP-liposomes, and liposomes with 1 mol% CPP and 5 mol% GCTE). Bars represent the mean ($n = 3$) \pm SEM.

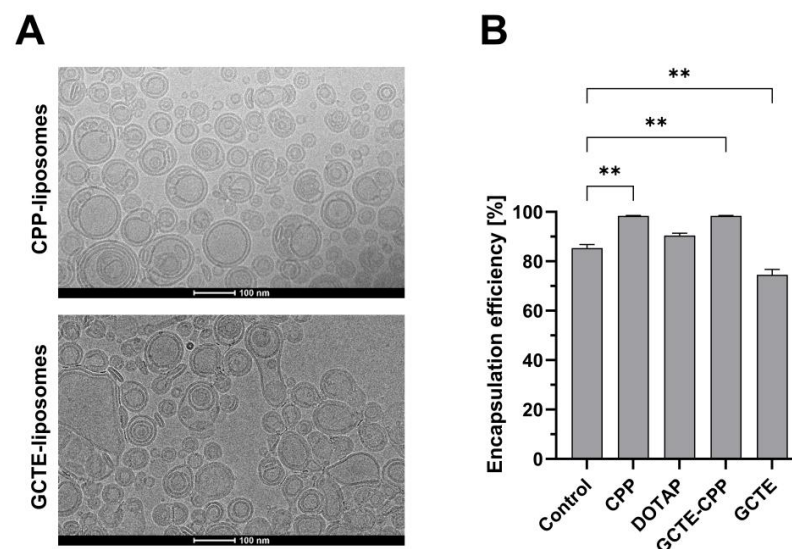


Figure 2. Structure, lamellarity, and encapsulation efficiency. (A) Cryogenic transmission electron microscopy images of CPP-liposomes and GCTE-liposomes containing 40 µg/mL GFP-mRNA. Scale bars represent 100 nm. (B) Encapsulation efficiency of liposomes containing 40 µg/mL GFP-mRNA. Bars represent the mean ($n = 2$) \pm SEM. Results were considered statistically significant at p value < 0.05 using a 95% confidence level (** for $p \leq 0.01$).

For cryo-TEM imaging, samples were shock-frozen. Since the structure and lamellarity of liposomes withstand shock-freezing, cryo-TEM images can be used to determine morphology [4,27,28]. Since only entrapped mRNA is protected from stress factors such as acidic pH in the stomach and enzymes in the GIT, the encapsulation efficiency was determined. Overall, encapsulation efficiencies of >70% were obtained. The highest encapsulation efficiencies were reached for GCTE-CPP-liposomes (98.5%) and CPP-liposomes (98.4%), followed by DOTAP-liposomes (90.5%), control liposomes (85.4%), and GCTE-liposomes (74.6%) (Figure 2B). Liposomes containing CPPs displayed significantly higher encapsulation efficiencies compared to control liposomes, while GCTE-liposomes entrapped significantly less mRNA. Higher encapsulation efficiencies were achieved in liposomal formulations with positive surface charges because positive components of liposomes enable the complexation of higher amounts of negatively charged mRNA.

Additionally, the stability of mRNA and liposomal formulations in simulated gastric (FaSSGF) and intestinal fluid (FaSSIF) was investigated. It could be demonstrated that non-encapsulated mRNA is steadily degraded under these conditions. The absence of free mRNA could be demonstrated for the CPP-liposomes in FaSSGF and FaSSIF. These findings indicate low release for this liposomal formulation (Figure S3). Stability of CPP-liposomes in FaSSIF with respect to size and PDI (Figure S4) could be demonstrated, while, in contrast, the PDI increased over time in FaSSGF.

3.3. Long-Term Storage Stability by Freeze-Drying

Long-term storage stability of the liposomes was achieved by freeze-drying the liposomes using 500 mM sucrose as a lyoprotectant. This concentration of sucrose was applied due to optimization in studies published previously [25,26]. As shown in Figure 3A, no significant changes were found in the liposomal size or PDI upon the addition of the lyoprotectant. Moreover, the liposome size and PDI were shown to be maintained during the freeze-drying process, indicating only a slight increase in size but a decrease in PDI, but all changes were not significant (Figure 3B). The lyophilizates had residual moisture below 5%, which is acceptable residual moisture for biological products and proves successful lyophilization [29]. To assess the long-term storage stability of liposomes, lyophilizates of freeze-dried liposomes were stored at -20°C , while liposome suspensions without freeze-drying were kept at room temperature for 2 months.

Overall, the liposomal particle sizes were maintained at the favorable size of <200 nm and a PDI < 0.3 during the 2 months of storage under both conditions, i.e., freeze-dried and without freeze-drying. Freeze-dried control liposomes and CPP-liposomes showed a slight increase in size after 2 months of storage (Figure 3C). CPP-liposomes demonstrated constant PDIs under freeze-dried conditions, and non-lyophilized CPP-liposomes showed an increase in PDI after 1 month, but this was not sustained after 2 months (Figure 3C). Freeze-dried DOTAP-liposomes showed increasing PDIs over the tested period and higher PDIs under non-lyophilized conditions, although the PDIs were still <0.3.

3.4. Cytotoxicity of Liposomal Formulations

Cytotoxicity assays showed that the addition of GFP-mRNA as well as the liposomal components GCTE, CPP, and DOTAP to empty control liposomes did not negatively affect cell viability compared to the positive control. As a positive control, the cells were incubated with medium, corresponding to 100% cell viability (Figure 4A). As a negative control, treatment of cells with 1% Triton X-100 was performed to lyse them. Additionally, liposomes were added at higher concentrations, diluted in medium without supplements instead of complete medium, and incubated for 24 h instead of 4 h to further evaluate cytotoxicity. Again, the liposomes showed no significant cytotoxic effects, except for the highest concentration of 40 mg/mL of CPP-liposomes, which resulted in a decrease in cell viability to 50% (Figure 4B). Lipofectamine, the positive control subsequently used in the uptake experiments, showed cell viability of about 100%. The positive influence

of medium supplements on cell viability was clearly demonstrated by the approximately twofold increase in cell viability compared with medium without supplements.

3.5. Uptake in Caco-2 Cells

Prior to in vivo application, cellular uptake in vitro was examined. Due to the assumption that the cell-penetrating peptides (which are positively charged) on the surface of liposomes might interact with components (negatively charged) of the intestinal mucosa and to increase cellular uptake, these experiments were performed with CPP-liposomes. The uptake of CPP-liposomes in Caco-2 cells was compared with cationic DOTAP-liposomes and control liposomes. The uptake was determined by quantitative fluorescence measurements. For this, the liposomal bilayer was modified with 1 mol% of a rhodamine-modified phospholipid, and fluorescently labeled GFP-mRNA was used to trace the cargo (AZDye488-labeled).

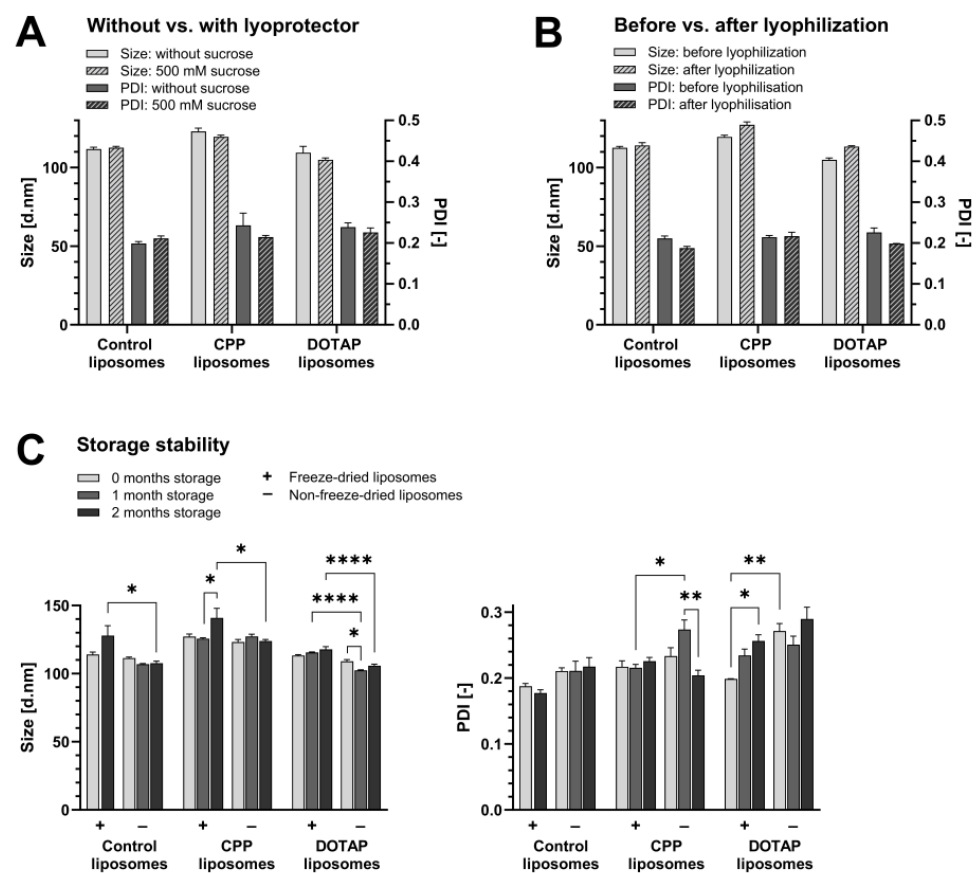


Figure 3. Long-term storage stability by freeze-drying. (A) Influence of lyoprotectant on liposomal characteristics: size (Z-average) and PDI of control liposomes, 1 mol% CPP-liposomes, and 5 mol% DOTAP-liposomes before and after the addition of the lyoprotectant, for which 500 mM sucrose was used. (B) Liposomal characteristics before and after lyophilization. Bars represent the mean ($n = 3$) \pm SEM. (C) Storage stability of liposomes: size and PDI of freeze-dried and non-freeze-dried control liposomes, 1 mol% CPP-liposomes, and 5 mol% DOTAP-liposomes after 0, 1, and 2 months of storage. Sucrose at a concentration of 500 mM was used as a lyoprotectant. Bars represent the mean ($n = 3$) \pm SEM; n.a. = not applicable. Results were considered statistically significant at p value < 0.05 using a 95% confidence level (* for $p \leq 0.05$; ** for $p \leq 0.01$; **** for $p \leq 0.0001$).

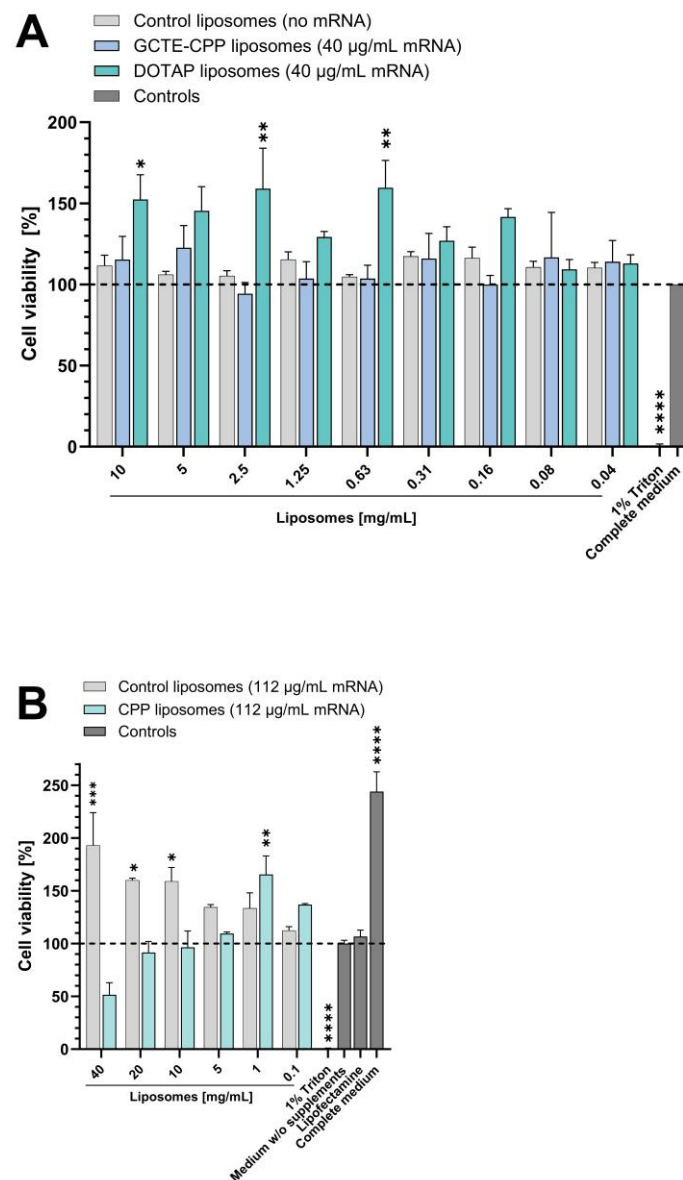


Figure 4. Cytotoxicity assays in which cells were incubated with (A) liposomes diluted in complete medium for 4 h and (B) liposomes diluted in medium without supplements for 24 h. Bars represent the mean ($n = 3$) \pm SEM. Results were considered statistically significant at p value < 0.05 using a 95% confidence level (* for $p \leq 0.05$; ** for $p \leq 0.01$; *** for $p \leq 0.001$; **** for $p \leq 0.0001$).

As shown in Figure 5A, incorporation of CPPs into liposomes significantly increases their uptake into cells. Here, the concentration of liposomes in cells was shown to increase with increasing treatment concentrations, whereas the highest measured intracellular concentration of CPP-liposomes was $0.72 \text{ mg/mL} \pm 0.00 \text{ mg/mL}$ (Figure 5B). In addition, the ratio of liposomes taken up (intracellular liposome concentration divided by extracellular liposome concentration after incubation) showed the highest uptake at the highest treatment concentration of 40 mg/mL CPP-liposomes, at which $16.6\% \pm 0.0\%$ of liposomes were taken up (Figure 5A). Since the cationic DOTAP-liposomes showed no measurable uptake, CPPs enable uptake into the cell not only by positively charging the liposomes but also by the functional structure of the CPPs themselves. Control liposomes showed no detectable uptake by Caco-2 cells. Despite attempts to optimize the uptake assay method, such as reducing the washing steps to spare cells, reducing the temperature for cell lysis to spare fluorescent labels of mRNA, increasing the concentration of mRNA in liposomes,

and reducing the background signal by removing cell debris, intracellular mRNA levels could not be quantified.

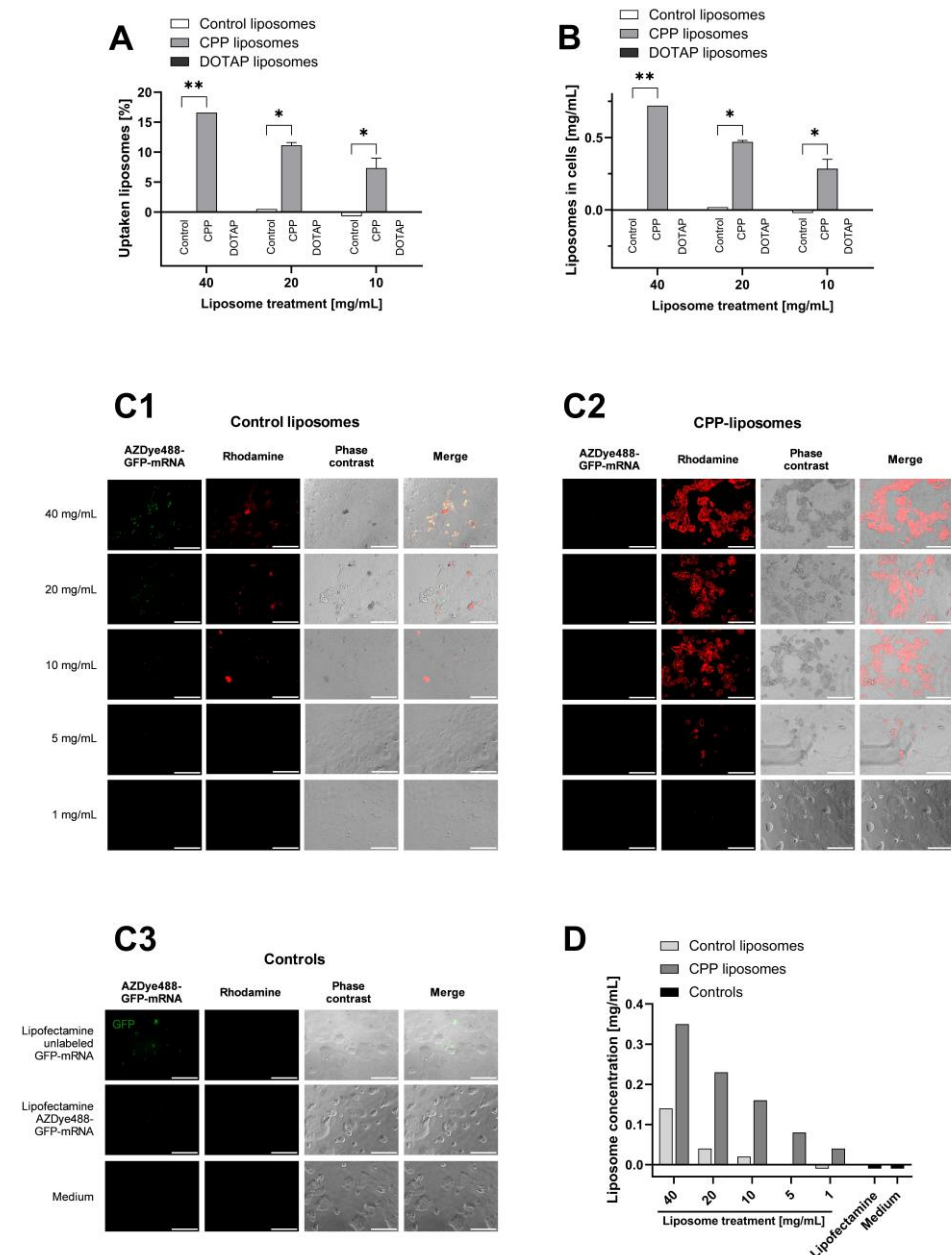


Figure 5. Uptake of liposomes in Caco-2 cells. (A) Percentage of liposomes that were taken up, and (B) concentration of intracellular liposomes. The uptake assay was performed according to method 1 (see methods—uptake). Bars of CPP-liposomes represent the mean ($n = 2$) \pm SEM. Experiments for control liposomes and DOTAP-liposomes were performed once. (C) Uptake assay: fluorescence microscopy images of Caco-2 cells treated with control liposomes (C1) and CPP-liposomes (C2) as well as indicated controls (C3). Liposomes contained 112 $\mu\text{g}/\text{mL}$ labeled GFP-mRNA. Images were acquired with exposure times of 1/25 s for AZDye488, 1/700 s for rhodamine in control liposomes and controls, and 1/3200 s for rhodamine in CPP-liposomes. Scale bars represent 200 μm . Images show representative cells from the respective conditions. (D) Uptake of liposomes from Caco-2 cells. Displayed is the concentration of intracellular liposomes. The uptake assay was performed according to method 2 (see methods—uptake) with the same samples used for microscopy. Results were considered statistically significant at p value < 0.05 using a 95% confidence level (* for $p \leq 0.05$; ** for $p \leq 0.01$).

Furthermore, fluorescence microscopy was performed to visualize the uptake, comparing CPP-liposomes and control liposomes. In accordance with the previous quantitative analysis, fluorescence microscopy images in Figure 5C show a significantly higher uptake of CPP-liposomes compared to control liposomes, recognizable by a stronger rhodamine signal. The intensity of the rhodamine signal decreases with a lower treatment concentration of control and CPP-liposomes. Unexpectedly, no mRNA was detected in cells incubated with CPP-liposomes. Potentially, the fluorescent dye could not be detected due to the interaction of CPP with the mRNA. The commercial transfection reagent Lipofectamine was used as a positive control. When the Lipofectamine particles were loaded with fluorescently labeled mRNA, punctate signals were seen showing the fluorescent tag. Lipofectamine was prepared without the addition of rhodamine and therefore showed no rhodamine signal. As expected, cells incubated with medium only do not show a signal at either 488 nm or for rhodamine. The merged images of control liposomes and CPP-liposomes showed cells with roughened and non-smooth surfaces, especially at the sites where liposomes are detected. The altered appearance of the cell surface could be due to the binding of liposomes. The samples used for microscopy were additionally evaluated quantitatively. For this, the fluorescent signals were read out using a plate reader without prior cell lysis since the Triton used for cell lysis interfered with the fluorescence mRNA measurements at 488 nm. Thus, without cell lysis, the determination of taken-up mRNA levels was aimed at. However, no conclusive results were obtained for the uptake of mRNA. The measured levels of the rhodamine signal shown in Figure 5D were consistent with the findings of the microscopic images, showing a clearly higher uptake by the incorporation of CPP into liposomes and demonstrating increasing intracellular liposome concentrations with higher liposome treatment concentrations. Again, no rhodamine signal was detected in cells incubated with Lipofectamine and medium.

4. Discussion

Despite great efforts to enable oral delivery of macromolecular therapeutics, few delivery systems have reached clinical phases in the past [30]. However, especially due to the development of the COVID-19 mRNA vaccines and the potential of nucleic acids as therapeutics, this goal has even become more important today. Up to now, there are few studies focusing on the successful oral delivery of nucleic acids [31,32]. Recently, a promising study has already been published focusing on local targeting in the intestine [33]. However, especially the impact of liposomal formulations to protect the encapsulated mRNA and facilitate intestinal uptake has not been evaluated in detail so far, while other routes of administration were comprehensively investigated [34–36]. Therefore, innovative, easy-to-administrate, and non-invasive oral formulations are still urgently required.

This study aimed to develop an easy-to-administrate liposomal formulation for increased oral uptake of mRNA *in vitro*. The liposomes obtained exhibit favorable properties for use as oral drug delivery systems. The particle sizes of <160 nm are in the desired range of <200 nm and comparable to previous studies using DAC as the preparation method, independent of the encapsulated drug [17,25]. Liposomes in this size range have been shown to be taken up quite well in cells [37]. In drug delivery applications using lipid-based carriers, such as liposome and nanoliposome formulations, a PDI of <0.3 is acceptable and indicates a homogenous population of particles [38,39]. Thus, the obtained narrow particle size distributions of <0.220 are also in the desired range, leading to better prediction of particle population behavior. In terms of surface charge, the highest uptake and/or surface binding to Caco-2 cells modeling the intestinal barrier was shown with cationic liposomes [40], making positively charged liposomes containing DOTAP and CPP most promising for later uptake experiments. Additional benefits of the CPP-liposomes could be demonstrated by obtaining the highest encapsulation efficiency of mRNA in comparison to other liposomal formulations (most probably due to charge interaction). As only liposomally encapsulated mRNA is protected from low pH and potential enzymatic degradation, the high encapsulation efficiency plays a key role in successful mRNA delivery.

Furthermore, the liposomes were successfully freeze-dried, and overall, their characteristics remained in the desired ranges over the 2-month period tested, as demonstrated previously for several liposomal formulations [25,26]. Although non-lyophilized liposomes exhibited only minor instability and their properties remained within the desired range of particle sizes < 200 nm and PDI < 0.3 during storage, non-lyophilized liposomes should not be hastily preferred. Not only does the stability of liposome particles represent a critical parameter for successful drug delivery, but the cargo, in this case, mRNA, must also be stable and remain encapsulated. To further evaluate the success of freeze-drying, the encapsulation efficiency after freeze-drying and the functionality of the mRNA should be determined. Freezing is currently the storage method of choice because mRNA was shown to be stable at -20°C . However, due to the increasing number of samples to be stored and the costly use of a cold chain, temperature preservation methods are becoming increasingly important [41,42].

As expected from previous studies with peptide therapeutics [25], CPP-liposomes showed an increased uptake of mRNA in Caco-2 cells compared to control liposomes and DOTAP-liposomes. However, in this assay, it is not possible to distinguish between uptake into the cell and binding to the cell. Thus, it remained unclear whether the liposomes and their cargo are really taken up into the cell or whether the liposomes only bind to the cell. This assay could also not clarify whether the loaded mRNA is released into the cell after uptake or binding or whether it remains in the liposomes. Therefore, additional investigations should be undertaken in subsequent studies.

5. Conclusions

In this study, mRNA-loaded liposomes could be prepared by DAC with favorable characteristics in terms of size, size distribution, surface charge, and encapsulation efficiency. The most favorable formulation (CPP-liposomes) was further shown to be non-cytotoxic on Caco-2 cells at relevant mRNA and lipid concentrations. Furthermore, these liposomes could be successfully freeze-dried, and subsequent long-term storage was accomplished. As a highlight, the CPP-liposomes were effectively taken up by Caco-2 cells, demonstrating that this liposomal drug delivery system could represent a promising tool for oral mRNA delivery.

Supplementary Materials: The following supporting information can be downloaded at: <https://www.mdpi.com/article/10.3390/applnano4040017/s1>, Figure S1: Size distribution by intensity of CPP-liposomes; Figure S2: Influence of mRNA loading on liposomal characteristics; Figure S3: Stability and release of mRNA out of liposomes in FaSSGF and FaSSIF; Figure S4: Stability of liposomal formulations in FaSSGF and FaSSIF.

Author Contributions: Conceptualization, W.M., G.F. and P.U.; methodology, V.D., G.F., W.M. and P.U.; formal analysis, V.D. and P.U.; investigation, V.D., S.W., T.E. and P.U.; resources, W.M., G.F. and P.U.; data curation, V.D. and P.U.; writing—original draft preparation, V.D. and P.U.; writing—review and editing, V.D., S.W., T.E., W.M., G.F. and P.U. All authors have read and agreed to the published version of the manuscript.

Funding: This research received no external funding.

Data Availability Statement: Data are contained within the article and in the Supplementary Materials (Figures S1–S4).

Acknowledgments: We thank Lipoid GmbH (Ludwigshafen, Germany) for the kind provision of lipids. Lipoid GmbH is further gratefully acknowledged for the endowment to the University of Heidelberg.

Conflicts of Interest: The authors declare no conflict of interest.

References

1. Saraf, S.; Jain, A.; Tiwari, A.; Verma, A.; Panda, P.K.; Jain, S.K. Advances in liposomal drug delivery to cancer: An overview. *J. Drug Deliv. Sci. Technol.* **2020**, *56*, 101549. [CrossRef]

2. Schoenmaker, L.; Witzigmann, D.; Kulkarni, J.A.; Verbeke, R.; Kersten, G.; Jiskoot, W.; Crommelin, D.J.A. mRNA-lipid nanoparticle COVID-19 vaccines: Structure and stability. *Int. J. Pharm.* **2021**, *601*, 120586. [[CrossRef](#)] [[PubMed](#)]
3. Yu, A.M.; Tu, M.J. Deliver the promise: RNAs as a new class of molecular entities for therapy and vaccination. *Pharmacol. Ther.* **2022**, *230*, 107967. [[CrossRef](#)] [[PubMed](#)]
4. Bibi, S.; Kaur, R.; Henriksen-Lacey, M.; McNeil, S.E.; Wilkhu, J.; Lattmann, E.; Christensen, D.; Mohammed, A.R.; Perrie, Y. Microscopy imaging of liposomes: From coverslips to environmental SEM. *Int. J. Pharm.* **2011**, *417*, 138–150. [[CrossRef](#)]
5. Tenchov, R.; Bird, R.; Curtze, A.E.; Zhou, Q. Lipid Nanoparticles-From Liposomes to mRNA Vaccine Delivery, a Landscape of Research Diversity and Advancement. *ACS Nano* **2021**, *15*, 16982–17015. [[CrossRef](#)] [[PubMed](#)]
6. Sastry, S.V.; Nyshadham, J.R.; Fix, J.A. Recent technological advances in oral drug delivery—A review. *Pharm. Sci. Technol.* **2000**, *3*, 138–145. [[CrossRef](#)]
7. Hamman, J.H.; Enslin, G.M.; Kotzé, A.F. Oral delivery of peptide drugs: Barriers and developments. *BioDrugs* **2005**, *19*, 165–177. [[CrossRef](#)]
8. Drucker, D.J. Advances in oral peptide therapeutics. *Nat. Rev. Drug Discov.* **2020**, *19*, 277–289. [[CrossRef](#)] [[PubMed](#)]
9. Choonara, B.F.; Choonara, Y.E.; Kumar, P.; Bijukumar, D.; Du Toit, L.C.; Pillay, V. A review of advanced oral drug delivery technologies facilitating the protection and absorption of protein and peptide molecules. *Biotechnol. Adv.* **2014**, *32*, 1269–1282. [[CrossRef](#)]
10. Wang, C.K.; Craik, D.J. Cyclic peptide oral bioavailability: Lessons from the past. *Biopolymers* **2016**, *106*, 901–909. [[CrossRef](#)]
11. Dunn, C.J.; Wagstaff, A.J.; Perry, C.M.; Plosker, G.L.; Goa, K.L. Cyclosporin: An updated review of the pharmacokinetic properties, clinical efficacy and tolerability of a microemulsion-based formulation (neoral)¹ in organ transplantation. *Drugs* **2001**, *61*, 1957–2016. [[CrossRef](#)]
12. Anderson, S.L.; Beutel, T.R.; Trujillo, J.M. Oral semaglutide in type 2 diabetes. *J. Diabetes Complicat.* **2020**, *34*, 107520. [[CrossRef](#)]
13. Melmed, S.; Popovic, V.; Bidlingmaier, M.; Mercado, M.; van der Lely, A.J.; Biermasz, N.; Bolanowski, M.; Coculescu, M.; Schopohl, J.; Raczyk, K.; et al. Safety and efficacy of oral octreotide in acromegaly: Results of a multicenter phase III trial. *J. Clin. Endocrinol.* **2015**, *100*, 1699–1708. [[CrossRef](#)]
14. Deshmukh, P.K.; Mutha, R.E.; Surana, S.J. Electrostatic deposition assisted preparation, characterization and evaluation of chrysin liposomes for breast cancer treatment. *Drug Dev. Ind. Pharm.* **2021**, *47*, 809–819. [[CrossRef](#)] [[PubMed](#)]
15. Jadhav, M.; Kalhapure, R.S.; Rambharose, S.; Mocktar, C.; Singh, S.; Kodama, T.; Govender, T. Novel lipids with three C18-fatty acid chains and an amino acid head group for pH-responsive and sustained antibiotic delivery. *Chem. Phys. Lipids.* **2018**, *212*, 12–25. [[CrossRef](#)] [[PubMed](#)]
16. Allen, T.M.; Cullis, P.R. Liposomal drug delivery systems: From concept to clinical applications. *Adv. Drug Deliv. Rev.* **2013**, *65*, 36–48. [[CrossRef](#)] [[PubMed](#)]
17. Uhl, P.; Helm, F.; Hofhaus, G.; Brings, S.; Kaufman, C.; Leotta, K.; Urban, S.; Haberkorn, U.; Mier, W.; Fricker, G. A liposomal formulation for the oral application of the investigational hepatitis B drug Myrcludex B. *Eur. J. Pharm. Biopharm.* **2016**, *103*, 159–166. [[CrossRef](#)]
18. Parmentier, J.; Hofhaus, G.; Thomas, S.; Cuesta, L.C.; Gropp, F.; Schröder, R.; Hartmann, K.; Fricker, G. Improved oral bioavailability of human growth hormone by a combination of liposomes containing bio-enhancers and tetraether lipids and omeprazole. *J. Pharm. Sci.* **2014**, *103*, 3985–3993. [[CrossRef](#)]
19. Swamynathan, S.K.; Wells, A. Conjunctival goblet cells: Ocular surface functions, disorders that affect them, and the potential for their regeneration. *Ocul. Surf.* **2020**, *18*, 19–26. [[CrossRef](#)]
20. Leal, J.; Dong, T.; Taylor, A.; Siegrist, E.; Gao, F.; Smyth, H.D.C.; Ghosh, D. Mucus-penetrating phage-displayed peptides for improved transport across a mucus-like model. *Int. J. Pharm.* **2018**, *553*, 57–64. [[CrossRef](#)]
21. Perez-Lopez, A.; Behnsen, J.; Nuccio, S.P.; Raffatellu, M. Mucosal immunity to pathogenic intestinal bacteria. *Nat. Rev. Immunol.* **2016**, *16*, 135–148. [[CrossRef](#)]
22. Chen, D.; Xia, D.; Li, X.; Zhu, Q.; Yu, H.; Zhu, C.; Gan, Y. Comparative study of Pluronic[®] F127-modified liposomes and chitosan-modified liposomes for mucus penetration and oral absorption of cyclosporine A in rats. *Int. J. Pharm.* **2013**, *449*, 1–9. [[CrossRef](#)] [[PubMed](#)]
23. Shan, W.; Zhu, X.; Liu, M.; Li, L.; Zhong, J.; Sun, W.; Zhang, Z.; Huang, Y. Overcoming the diffusion barrier of mucus and absorption barrier of epithelium by self-assembled nanoparticles for oral delivery of insulin. *ACS Nano* **2015**, *9*, 2345–2356. [[CrossRef](#)] [[PubMed](#)]
24. Uhl, P.; Grundmann, C.; Sauter, M.; Storck, P.; Tursch, A.; Özbek, S.; Leotta, K.; Roth, R.; Witzigmann, D.; Kulkarni, J.A.; et al. Coating of PLA-nanoparticles with cyclic, arginine-rich cell penetrating peptides enables oral delivery of liraglutide. *Nanomed. Nanotechnol. Biol. Med.* **2020**, *24*, 102132. [[CrossRef](#)]
25. Uhl, P.; Sauter, M.; Hertlein, T.; Witzigmann, D.; Laffleur, F.; Hofhaus, G.; Fidelj, V.; Tursch, A.; Özbek, S.; Hopke, E.; et al. Overcoming the Mucosal Barrier: Tetraether Lipid-Stabilized Liposomal Nanocarriers Decorated with Cell-Penetrating Peptides Enable Oral Delivery of Vancomycin. *Adv. Therap.* **2021**, *4*, 000247. [[CrossRef](#)]
26. Uhl, P.; Pantze, S.; Storck, P.; Parmentier, J.; Witzigmann, D.; Hofhaus, G.; Huwyler, J.; Mier, W.; Fricker, G. Oral delivery of vancomycin by tetraether lipid liposomes. *Eur. J. Pharm. Sci.* **2017**, *108*, 111–118. [[CrossRef](#)] [[PubMed](#)]
27. Kuntsche, J.; Horst, J.C.; Bunjes, H. Cryogenic transmission electron microscopy (cryo-TEM) for studying the morphology of colloidal drug delivery systems. *Int. J. Pharm.* **2011**, *417*, 120–137. [[CrossRef](#)] [[PubMed](#)]

28. Weisman, S.; Hirsch-Lerner, D.; Barenholz, Y.; Talmon, Y. Nanostructure of cationic lipid-oligonucleotide complexes. *Biophys. J.* **2004**, *87*, 609–614. [[CrossRef](#)]
29. Fahr, A.; Voigt, R. *Voigt Pharmazeutische Technologie. Für Studium und Beruf*, 12th ed.; Völlig Neu Bearb. Aufl. Stuttgart; Deutscher Apotheker Verlag (Wissen und Praxis): Stuttgart, Germany, 2015; ISBN 978-3-7692-6194-3.
30. Goldberg, M.; Gomez-Orellana, I. Challenges for the oral delivery of macromolecules. *Nat. Rev. Drug Discov.* **2003**, *2*, 289–295. [[CrossRef](#)]
31. Abramson, A.; Kirtane, A.R.; Shi, Y.; Zhong, G.; Collins, J.E.; Tamang, S.; Ishida, K.; Hayward, A.; Wainer, J.; Rajesh, N.U.; et al. Oral mRNA delivery using capsule-mediated gastrointestinal tissue injections. *Matter* **2022**, *5*, 975–987. [[CrossRef](#)]
32. Tao, W.; Peppas, N.A. Robotic pills for gastrointestinal-tract-targeted oral mRNA delivery. *Matter* **2022**, *5*, 775–777. [[CrossRef](#)]
33. Sung, J.; Alghoul, Z.; Long, D.; Yang, C.; Merlin, D. Oral delivery of IL-22 mRNA-loaded lipid nanoparticles targeting the injured intestinal mucosa: A novel therapeutic solution to treat ulcerative colitis. *Biomaterials* **2022**, *288*, 121707. [[CrossRef](#)] [[PubMed](#)]
34. Mai, Y.; Guo, J.; Zhao, Y.; Ma, S.; Hou, Y.; Yang, J. Intranasal delivery of cationic liposome-protamine complex mRNA vaccine elicits effective anti-tumor immunity. *Cell. Immunol.* **2020**, *354*, 104143. [[CrossRef](#)] [[PubMed](#)]
35. Dhaliwal, H.K.; Fan, Y.; Kim, J.; Amiji, M.M. Intranasal delivery and transfection of mRNA therapeutics in the brain using cationic liposomes. *Mol. Pharm.* **2020**, *17*, 1996–2005. [[CrossRef](#)]
36. Huang, H.; Zhang, C.; Yang, S.; Xiao, W.; Zheng, Q.; Song, X. The investigation of mRNA vaccines formulated in liposomes administrated in multiple routes against SARS-CoV-2. *J. Control. Release* **2021**, *335*, 449–456. [[CrossRef](#)] [[PubMed](#)]
37. He, H.; Lu, Y.; Qi, J.; Zhu, Q.; Chen, Z.; Wu, W. Adapting liposomes for oral drug delivery. *Acta Pharm. Sin. B* **2019**, *9*, 36–48. [[CrossRef](#)]
38. Chen, M.; Liu, X.; Fahr, A. Skin penetration and deposition of carboxyfluorescein and temoporfin from different lipid vesicular systems: In vitro study with finite and infinite dosage application. *Int. J. Pharm.* **2011**, *408*, 223–234. [[CrossRef](#)] [[PubMed](#)]
39. Putri, D.C.A.; Dwiastuti, R.; Marchaban, M.; Nugroho, A.K. Optimization of mixing temperature and sonication during liposome preparation. *J. Pharm. Sci. Community* **2017**, *14*, 79–85. [[CrossRef](#)]
40. Kono, Y.; Iwasaki, A.; Fujita, T. Effect of surface charge, particle size, and modification by polyethylene glycol of liposomes on their association with Caco-2 cells across an unstirred water layer. *Die Pharm.* **2018**, *73*, 3–8. [[CrossRef](#)]
41. Fabre, A.L.; Colotte, M.; Luis, A.; Tuffet, S.; Bonnet, J. An efficient method for long-term room temperature storage of RNA. *Eur. J. Hum. Genet.* **2014**, *22*, 379–385. [[CrossRef](#)]
42. Oude Blenke, E.; Örnkov, E.; Schöneich, C.; Nilsson, G.A.; Volkin, D.B.; Mastrobattista, E.; Almarsson, Ö.; Crommelin, D.J.A. The Storage and In-Use Stability of mRNA Vaccines and Therapeutics: Not A Cold Case. *J. Pharm. Sci.* **2022**, *112*, 386–403. [[CrossRef](#)] [[PubMed](#)]

Disclaimer/Publisher’s Note: The statements, opinions and data contained in all publications are solely those of the individual author(s) and contributor(s) and not of MDPI and/or the editor(s). MDPI and/or the editor(s) disclaim responsibility for any injury to people or property resulting from any ideas, methods, instructions or products referred to in the content.